Near-field analysis of the knife-edge technique

Abraham Aharoni, Abraham Gover, and Kenneth M. Jassby

While employing the knife-edge (KE) technique for detecting surface acoustic waves (SAW) in an experimental apparatus, it was observed that the phase of the detected signals varied with the lateral position of the KE. This phenomenon is explained by deriving the Fresnel diffraction pattern of a Gaussian beam reflected from a surface sustaining continuous SAW and applying the results to obtain an analytical expression for the signal detected by the KE technique in the near-field. The dependence of the detected acoustic signal on the lateral position of the KE, which is described by this expression, is verified experimentally. The frequency response of the KE technique and the effect of nonsinusoidal SAW are also considered.

I. Introduction

The detailed analysis presented here was motivated by an experimental observation noted by the authors while attempting to measure the phase of surface acoustic waves (SAW) by means of the knife-edge (KE) technique.[1-4] The authors found that the phase of the detected acoustic signals depended on the lateral position of the KE. This dependence persisted when the KE was placed well within the far-field region as defined by the standard condition[1-4] $z \gg W_1^2/\lambda$, where z is the distance from the surface sustaining SAW, W_1 is the extent of the illuminated spot on the surface, and λ is the optical wavelength. This phenomenon is not predicted by theoretical analyses of the KE technique for the far-field, and its occurrence may hinder the applicability of the KE techniques in situations where the detected phase is significant, such as SAW velocity measurements by the time-of-flight technique.[5] Using the near-field diffraction approach it is possible to explain this phase variation and define a confined region within the far-field where this phenomenon is negligible.

The reader is referred to Refs. 1–4 for detailed analyses of the KE technique. A short geometrical optics description of this technique follows. In its simplest experimental form (shown schematically in Fig. 1), the KE technique comprises a lens which is used to focus the incident beam onto the material surface and a KE which is placed in the path of the reflected beam, blocking half of it when the material surface is unperturbed. If SAW are introduced to the material surface, the reflected beam experiences a periodic deflection due to the tilting of the material surface at the point of illumination [as shown in Fig. 2(b)]. The resulting variation in light intensity behind the KE [as shown in Fig. 2(a)] is transduced into an equivalent electronic signal by a photodetector.

The Fresnel diffraction pattern of a Gaussian beam reflected from a surface sustaining SAW is derived in Sec. II and employed in Sec. III for deriving an analytical expression for the detected signal in the KE technique. The resulting expression for the detected signal describes a dependence of the signal phase on the KE position closely resembling experimental results (presented in Sec. VII). In Sec. IV the variation of the detected signal power with the extent of the illuminating spot W_1 is considered. This effect is found to result in the bandpass frequency selectivity of the KE detection when the initial near-field analysis is extended in Sec. V to describe nonsinusoidal SAW. In Sec. VI the results of Sec. III are modified to include the effect of a lens system placed in the optical beam path.

II. Gaussian Beam Diffracted by Continuous SAW

In this section we will assume an optical Gaussian beam incident on a SAW propagating surface and apply the Fresnel diffraction integral approximation to obtain the near-field diffraction pattern. Although the formal derivation of the Fresnel approximation limits the optical aperture W with respect to the distance to the observation plane z so that $W \ll z$, it has been shown that it is valid even for $W \simeq z$.[6] This condition poses essentially no limitations on the applicability of the following derivation for describing any practical experimental situation.

The authors are with Tel-Aviv University, School of Engineering, Ramat-Aviv, 69978 Tel-Aviv, Israel.

Received 26 November 1984.
0003-6935/85/183018-10$02.00/0.

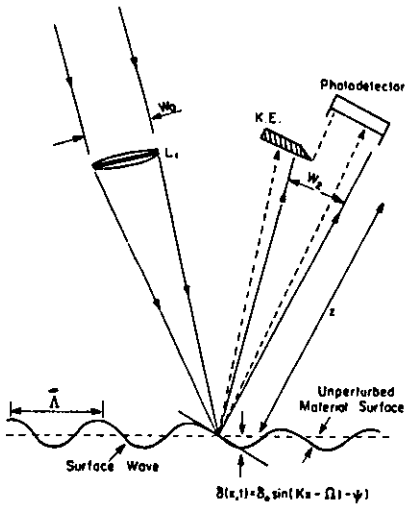

Fig. 1. Schematic illustration of the KE technique.

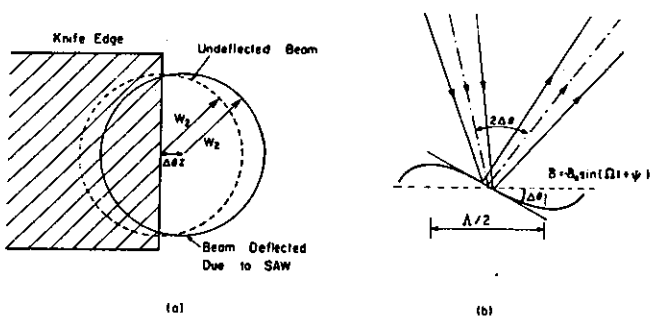

Fig. 2. Deflected beam geometry in the KE technique. Cross-sectional view of the KE (a) and side view of the material surface (b).

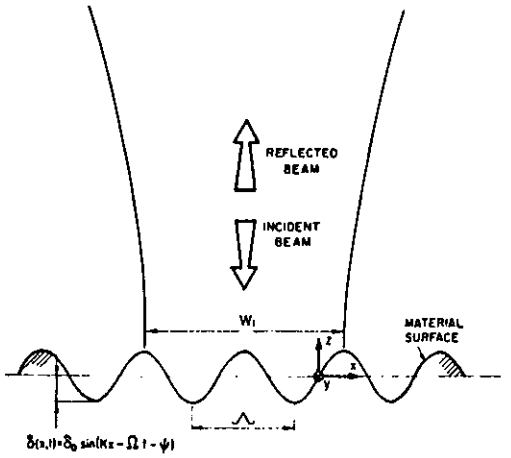

Fig. 3. Schematic illustration of a light beam reflected off a surface sustaining SAW.

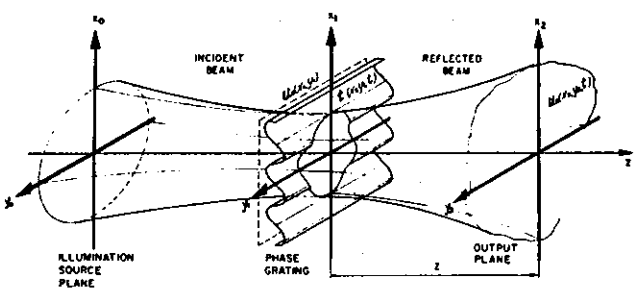

Fig. 4. Schematic illustration of a light beam modulated by SAW.

For clarity the actual reflection geometry of the KE technique shown in Fig. 3 is transformed to the transmission geometry of Fig. 4, where the modulation of the incident light beam by the SAW is represented by an hypothetical transmission function $t(x_1,t)$. The field at a distance z from the SAW propagating surface may be found by the Fresnel diffraction integral

$$U_2(x_2,y_2,t) = \frac{\exp(ikz)}{i\lambda z}\iint_{-\infty}^{\infty} U_0(x_1,y_1,t)t(x_1,t) \times \exp\left\{\frac{ik}{2z}[(x_2-x_1)^2+(y_2-y_1)^2]\right\}dx_1dy_1, \quad (1)$$

where k and λ are the optical wave number and wavelength, respectively. Here we shall assume an incident Gaussian beam which has the following amplitude distribution[7]:

$$U_0(x_1,y_1,t) = E_0\frac{W_0}{W_1}\exp\left[-\frac{1}{W_1^2}(x_1^2+y_1^2) + \frac{ik}{2r_1}(x_1^2+y_1^2)\right]\exp(-i\omega t - i\phi), \quad (2)$$

where W_1 is the $1/e^2$ power width of the beam, r_1 is the effective radius of phase curvature, ω is the optical frequency, and ϕ is a constant optical phase shift. The effective radius of phase curvature of the Gaussian beam at the surface r_1 includes the effect of any lens system in the incident or reflected optical paths (see Sec. VI).

For the case of SAW propagating on a reflective surface, the incident light is phase modulated by the surface ripple introduce by the SAW to the surface. The surface ripple due to a single-frequency SAW component of vertical displacement amplitude δ_0 (in the z direction), frequency Ω, wave number κ, and phase ψ,[8]

$$\delta(x,t) = \delta_0\sin(\kappa x - \omega t - \psi), \quad (3)$$

introduces in the optical beam a phase modulation

$$t(x_1,t) = R\exp[i2k\delta_0\sin(\kappa x_1 - \omega t - \psi)]. \quad (4)$$

R, the reflection coefficient of the material, is assumed throughout this work to be real.

This transmission function and consequent analysis are similar to those found in the case of a conventional phase grating.[9] However, the time dependence of the transmission function here requires that it be first expanded into temporal spectral components to comply with the diffraction integral. This is done by applying the identity[10]

$$\exp(ia\sin\theta) = \sum_{q=-\infty}^{\infty} J_q(a)\exp(iq\theta), \quad (5)$$

where J_q is the Bessel function of the first kind, order q. Thus the transmission function $t(x_1,t)$ of Eq. (4) becomes

$$t(x_1,t) = R \sum_{q=-\infty}^{\infty} J_q(2k\delta_0) \exp[iq(\kappa x_1 - \Omega t - \psi)],$$

so that

$$U_1(x_1,y_1,t) = U_0(x_1,y_1,t)t(x_1,t) = RE_0 \frac{W_0}{W_1} \sum_{q=-\infty}^{\infty} U_{1,q}(x_1,y_1,t), \quad (6)$$

where

$$U_{1,q}(x_1,y_1,t) = J_q \exp\left[-\frac{1}{W_1^2}(x_1^2+y_1^2) + \frac{ik}{2r_1}(x_1^2+y_1^2) + iq(\kappa x_1 - \psi)\right] \times \exp[-i(q\Omega+\omega)t - i\phi], \quad (6a)$$

and

$$J_q = J_q(2k\delta_0). \quad (6b)$$

The terms $U_{1,q}(x_1,y_1,t)$ in Eq. (6a) are the single-frequency components of the optical field immediately on reflection. Each diffracted optical field component, $U_{2,q}(x_2,y_2,t)$, is found by Fresnel integration of the corresponding component in the (x_1,y_1) plane, $U_{1,q}(x_1,y_1,t)$, that is,

$$U_{2,q}(x_2,y_2,t) = \frac{J_q \exp(ik_q z)}{i\lambda_q z} \iint_{-\infty}^{\infty} U_{1,q}(x_1,y_1,t) \times \exp\left\{i\frac{k_q}{2z}[(x_2-x_1)^2+(y_2-y_1)^2]\right\} dx_1 dy_1, \quad (7)$$

where λ_q is the optical wavelength of the qth order corresponding to the frequency $\omega + q\Omega$. Substituting for $U_{1,q}(x_1,y_1,t)$ from Eq. (6a), terms containing the x_1 and y_1 integration variables in Eq. (7) can be separated to give

$$U_{2,q}(x_2,y_2,t) = \frac{J_q}{i\lambda_q z} \exp(ik_q z - i\phi) \exp\left[\frac{ik_q}{2z}(x_2^2+y_2^2)\right] \times \exp[-i(q\Omega+\omega)t - iq\psi]\mathcal{I}_q(x_2)\mathcal{J}_q(y_2), \quad (8)$$

where

$$\mathcal{I}_q(x_2) = \int_{-\infty}^{\infty} \exp\left(-\frac{x_1^2}{W_1^2} + \frac{ik_q}{2r_1}x_1^2 + iq\kappa x_1 + i\frac{k_q}{2z}x_1^2 - i\frac{k_q}{z}x_1x_2\right) dx_1, \quad (8a)$$

$$\mathcal{J}_q(y_2) = \int_{-\infty}^{\infty} \exp\left(-\frac{y_1^2}{W_1^2} + \frac{ik_q}{2r_1}y_1^2 + i\frac{k_q}{2z}y_1^2 - i\frac{k_q}{z}y_1y_2\right) dy_1. \quad (8b)$$

Formally k_q and λ_q are functions of q, that is,

$$k_q = \frac{\omega_q}{c} = \frac{\omega + q\Omega}{c} = k\left(1 + q\frac{\Omega}{\omega}\right),$$

where c is the speed of light. However, the typical magnitudes of Ω and ω are 10^6 and 10^{15} Hz, respectively, so that, for any practical considerations, the difference between k and k_q is minute and, therefore, ignored.

Equations (8a) and (8b) may be evaluated by employing the integral identity[10]

$$\int_{-\infty}^{\infty} \exp(-\gamma x^2 + i\beta x^2 + 2i\xi x)dx = \frac{\sqrt{\pi}}{\sqrt{\gamma^2+\beta^2}} \exp\left[\frac{i}{2}\arctan(\beta/\gamma) - \frac{\gamma+i\beta}{\gamma^2+\beta^2}\xi^2\right]. \quad (9)$$

Each diffracted frequency component may be eventually reduced to the form[5]

$$U_{2,q}(x_2,y_2,t) = J_q \exp\left\{-\frac{1}{W_2^2}[(x_2-q\Delta x)^2+y_2^2] + \frac{ik}{2r_2}(x_2^2+y_2^2) + iqg\left(x_2 - q\frac{\Delta x}{2}\right)\right\} \times \exp[-i(q\Omega+\omega)t - iq\psi + i\Phi], \quad (10)$$

where the following parameters have been defined:

$$W_2 = W_1\sqrt{\zeta^2 + z^2/Z^2}, \quad (10a)$$

$$Z = (\pi W_1^2)/\lambda, \quad (10b)$$

$$\zeta = 1 + z/r_1, \quad (10c)$$

$$\frac{1}{r_2} = \frac{1}{z}\left[1 - \frac{\zeta}{\zeta^2 + (z/Z)^2}\right], \quad (10d)$$

$$\Delta x = \frac{\kappa}{k}z = \frac{\lambda}{\Lambda}z, \quad (10e)$$

$$g = \kappa(1 - z/r_2). \quad (10f)$$

In Eq. (10e) Λ denotes the acoustic wavelength and the constant phase in Eq. (10) Φ includes all the phase terms at the distance z in the absence of SAW.

The final expression for the diffracted field, $U_2(x_2,y_2,t)$, is found by summing over all q orders, that is,

$$U_2(x_2,y_2,t) = RE_0 \frac{W_0}{W_2} \sum_{q=-\infty}^{\infty} U_{2,q}(x_2,y_2,t). \quad (11)$$

This result has a number of interesting features. For the qth order, the frequency of the diffracted light is shifted by $q\Omega$ from the incident light frequency. Each order has a Gaussian amplitude distribution with $1/e^2$ power width W_2 and phase curvature $1/r_2$, and each is shifted in space from the $q = 0$ order beam $q\Delta x = q(\lambda/\Lambda)z$. Physically, Eq. (11) may be interpreted as an infinite sum of Gaussian beams with the qth beam tilted in space at the diffraction angle $q(\lambda/\Lambda)$. The term linear in x_2 in the exponential, $qg\{x_2 - q[(\Delta x)/2]\}$, which appears in each diffracted order, results from the fact that the direction of propagation of each diffracted order is tilted with respect to the coordinate system.

The near-field diffraction pattern of Eq. (11) bears a resemblance to the far-field pattern normally associated with the diffraction of a Gaussian beam from SAW.[11] Indeed Eq. (11) reduces to the far-field diffraction pattern when the far-field conditions, $z \to \infty$ or $r_2 \to \infty$, implying $W_2 \to (\lambda z)/(\pi W_1)$ and $g \to 0$, are imposed. The most significant difference between the near- and far-field patterns is the spatial variation of each order's optical phase which is found in the near-field but completely eliminated in the far-field. Consequently, the observed intensity distributions of the diffracted light may be substantially different in the two regimens.

III KE Technique—a Fresnel Analysis

The result of the previous section is employed in the following to analyze the KE system of Fig. 1. In Sec. VI it will be shown that the treatment developed here re-

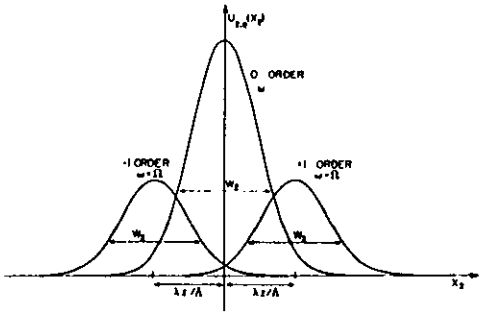

Fig. 5. First three diffraction orders for $W_1 < \Delta x$.

mains valid for any additional lens system incorporated into the simple KE arrangement of Fig. 1.

The Bessel functions of Eq. (10), J_q, have arguments, $2k\delta_0$, which are, for light modulated by SAW, typically no larger than 10^{-3}, so that J_q for $q > 1$ is negligibly small, and the infinite sum in Eq. (11) may be approximated by

$$U_2(x_2,y_2,t) \simeq RE_0 \frac{W_0}{W_2}(U_{2,-1} + U_{2,0} + U_{2,1}). \tag{12}$$

In the KE technique, the beam spot width W_1 is expected to be smaller than $\Lambda/2$, so that the separation between orders, $(\lambda/\Lambda)z$, is normally smaller than their width

$$W_2 \geq W_1 \frac{\lambda z}{\pi W_1^2} \geq \frac{2\lambda z}{\pi \Lambda}.$$

This condition is obtained directly from Eq. (10a). Therefore, the $q = 0, \pm 1$ diffraction orders are to a large extent overlapped, as shown schematically in Fig. 5.

Both the $q = 1$ and $q = -1$ orders, which oscillate at frequencies $\omega + \Omega$ and $\omega - \Omega$, respectively, heterodyne with the $q = 0$ order, producing rf signals at a frequency Ω. These two rf signals are equal in amplitude and 180° out of phase and would, therefore, cancel one another if all 3 orders were allowed to impinge on the same photodetector. However, a KE manipulated in the (x_2,y_2) plane to block one-half of the $q = 0$ order diffraction beam will in addition block a larger part of the $q = -1$ order beam, say, than of the $q = +1$ order beam, depending on their positions relative to the KE. The resulting out-of-phase rf signals which are produced by the unblocked portions of the +1 and −1 optical orders will be of differrent amplitudes, and a net electronic signal will develop on the photodetector.

This qualitative wave optics interpretation of the KE technique is quantified in the following. The total diffracted beam power density may be approximated by

$$P_2 = \frac{1}{2}\sqrt{\frac{\epsilon}{\mu}} U_2 U_2^*$$
$$= \frac{1}{2}\sqrt{\frac{\epsilon}{\mu}} R^2 |E_0|^2 \left(\frac{W_0}{W_2}\right)^2 (U_{2,0}U_{2,1}^* + U_{2,0}U_{2,0}^* + U_{2,0}U_{2,1}^* + \text{c.c.}) \tag{13}$$

where ϵ and μ are, respectively, the permittivity and permeability of the light propagating medium and where the small cross-terms have been neglected. Using the expression for the incident power,

$$P_0 = \frac{\pi}{4}\sqrt{\frac{\epsilon}{\mu}} |E_0|^2 W_0^2,$$

the optical power density distribution associated with the Ω heterodyne frequency component may be written as

$$P_{2,\Omega}(x_2,y_2,t) = \frac{2R^2P_0}{\pi W_2^2}[U_{2,0}(U_{2,-1}^* + U_{2,+1}^*) + \text{c.c.}]. \tag{14}$$

Employing Eq. (11), using the identity $J_{-1} = -J_1$ and expressing the sums of conjugate imaginary exponents in cosine form, the time-dependent total power density distribution can be expressed as

$$P_{2,\Omega}(x_2,y_2,t) = \frac{2R^2P_0}{\pi W_2^2} J_0 J_1 \exp\left(-\frac{x_2^2 + 2y_2^2}{W_2^2}\right)$$
$$\times \left\{\exp\left[-\frac{(x_2 - \Delta x)^2}{W_2^2}\right] \cos\left[+\Omega t + \psi - g\left(x_2 - \frac{\Delta x}{2}\right)\right]\right.$$
$$\left. - \exp\left[-\frac{(x_2 + \Delta x)^2}{W_2^2}\right] \cos\left[-\Omega t - \psi + g\left(x_2 + \frac{\Delta x}{2}\right)\right]\right\}. \tag{15}$$

This expression for the Ω frequency component of the optical irradiance distribution differs from the expression for the irradiance distribution in the far-field, which was derived by other workers.[2] The present result is more general since it applies for both far- and near-field regions and includes the effects of any lens system in the optical path (see Sect. VI). Equation (15) differs from the far-field expression mainly in the dependence of the rf signal phase on the spatial component x_2. This dependence is shown below to result in a dependence of the electronic signal phase on KE position, similar to the experimental observations described in Sec. VII. That is, the phase at which the SAW is detected depends on the lateral position of the KE. It was shown in Sec. II that in the far-field limit, $g = 0$, and this phase dependence vanishes in accordance with the standard far-field result.[2]

The total optical signal measured at the photodiode surface is found by integrating $P_{2,\Omega}(x_2,y_2,t)$ in Eq. (15) over the area of the unblocked diffracted beam in the plane of the knife-edge. That is

$$P_{\text{sig}}(x_d,t) = \int_{x_d}^{\infty} dx_2 \int_{-\infty}^{\infty} dy_2 P_{2,\Omega}(x_2,y_2,t), \tag{16}$$

where $x_2 = x_d$ marks the position of the KE as imaged or projected on the photodetector. On evaluating the integral over y_2, Eq. (16) is reduced to the form

$$P_{\text{sig}}(x_d,t) = \sqrt{\frac{2}{\pi}} \frac{R^2P_0}{W_2} J_0 J_1 \mathcal{J}_{\text{sig}}(x_d,t), \tag{17}$$

where

$$\mathcal{J}_{\text{sig}}(x_d,t) = \int_{x_d}^{\infty} \left\{\exp\left[-\left(\frac{x_2}{W_2}\right)^2 - \left(\frac{x_2 - \Delta x}{W_2}\right)^2\right]\right.$$
$$\times \cos\left[\Omega t + \psi - g\left(x_2 - \frac{\Delta x}{2}\right)\right]$$
$$- \exp\left[-\left(\frac{x_2}{W_2}\right)^2 - \left(\frac{x_2 + \Delta x}{W_2}\right)^2\right]$$
$$\left.\times \cos\left[\Omega t + \psi - g\left(x_2 + \frac{\Delta x}{2}\right)\right]\right\} dx_2. \tag{17a}$$

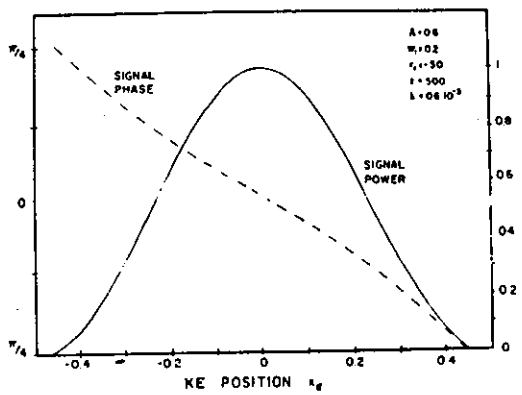

Fig. 6. Amplitude and phase variations of the signal power as a function of x_d.

A more symmetric expression for the signal power is obtained by substituting $x' = x_2 - \frac{1}{2}\Delta x$ and $x'' = x_2 + \frac{1}{2}\Delta x$ in the first and second terms of Eq. (10a), respectively,

$$\mathcal{J}_{sig}(x_d,t) = \exp\left[-\frac{1}{2}\left(\frac{\Delta x}{W_2}\right)^2\right]\int_{x_d-\Delta x/2}^{x_d+\Delta x/2} dx \times \exp\left[-2\left(\frac{x}{W_2}\right)^2\right]\cos(\Omega t + \psi - gx). \quad (18)$$

This form is particularly useful as it demonstrates that $\mathcal{J}_{sig}(x_d,t) \to 0$ as $x_d \to \infty$, that is, no net signal will be obtained in the absence of a KE. The integral in Eq. (18) was evaluated numerically and typical results are presented in Fig. 6. For small values of Δx this expression may be approximated by

$$\mathcal{J}_{sig}(x_d,t) \simeq \Delta x \exp\left[-\frac{1}{2}\left(\frac{\Delta x}{W_2}\right)^2\right]\exp\left[-2\left(\frac{x_d}{W_2}\right)^2\right]\cos(\Omega t + \psi - gx_d).$$

In this case the total signal power [Eq. (17)] is given by

$$P_{sig}(x_d,t) = \sqrt{\frac{2}{\pi}}R^2P_0J_0J_1\frac{\Delta x}{W_2}\exp\left(-\frac{4x_d^2+\Delta x^2}{2W_2^2}\right) \times \cos(\Omega t + \psi - gx_d), \quad (19)$$

where, as previously noted, the phase of the detected acoustic signal depends on the spatial position of the KE x_d.

Physically this phenomenon may be understood in a partial imaging context. The diffraction pattern in any particular plane in the near-field region displays a geometric correspondence between regions in this plane and limited regions on the illuminated reflecting material surface. As a result each spatial region exhibits the phase of a different point on the SAW path. This behavior may be demonstrated by showing that the total phase change $\Delta\Psi_{max}$ across the width of the diffraction pattern W_2 is related to the acoustic phase difference across the width of the illuminating spot. The maximal phase shift is obtained for $\Delta x_d = W_2$. Hence

$$\Delta\Psi_{max} = -gW_2 = 2\pi\frac{W_1}{\Lambda}\left(\frac{1}{r_1}+\frac{1}{z}\right)\left[\left(\frac{\lambda z}{\pi W_1^2}\right)^2+\left(\frac{1}{r_1}+\frac{1}{z}\right)^2\right]^{-1/2}.$$

In the extreme case for which $z \to 0$, $\Delta\Psi_{max} \to -2\pi(W_1/\Lambda)$, and the phase change has a 1:1 correspondence to the SAW surface path. For $z \to \infty$ and $r_1 \to \infty$, $\Delta\Psi_{max} \to 0$, so the far-field condition of no spatial phase dependence implied in the literature[2] is verified. Between these extremes the spatial phase dependence gradually decreases as the observed diffraction plane draws further from the SAW surface.

In concluding the present section, signal power results for the geometrical optics and Fresnel analyses are compared. In setting $x_d = 0$ the signal power obtained by the Fresnel analysis [Eq. (19)] reduces to

$$P_{sig}(t) = \sqrt{\frac{2}{\pi}}\frac{\Delta x}{W_2}R^2J_0J_1P_0\exp\left[-\frac{1}{2}\left(\frac{\Delta x}{W_2}\right)^2\right]\cos(\Omega t + \psi) \simeq \sqrt{\frac{2}{\pi}}R^2P_0(z\theta_{beam})^{-1}k\delta_0\frac{\lambda}{\Lambda}z\cos(\Omega t + \psi),$$

where the small argument approximations for the Bessel functions are used, the far-field approximation

$$W_2 \simeq z\theta_{beam} = z\frac{2\lambda}{\pi W_1}$$

for a coherent Gaussian wave is applied,[7] and $\Delta x \ll W_2$ is assumed. For these conditions

$$P_{sig}(t) = \sqrt{2\pi}\frac{\pi W_1}{\Lambda}\frac{\delta_0}{\lambda}R^2P_0\cos(\Omega t + \psi), \quad (20)$$

which is, as expected, proportional to the derivative of the acoustic waveform at $x = 0$ [Eq. (3)]. The result in Eq. (20) exhibits the same parameter dependence as that obtained in Ref. 2 for a uniform square spot illumination. The different scaling factors, $\sqrt{2\pi}$ in Eq. (20) and 4 in Ref. 2, indicate a reduced detection sensitivity with Gaussian beam illumination compared with the sensitivity possible with uniform square illumination (see Sec. IV where the beamwidth for maximal sensitivity for Gaussian illumination is found to be smaller than that for uniform illumination).

IV. Beamwidth for Maximal Signal

The beamwidth which maximizes the detected signal is predicted in this section, offering further insight into the detection process. The value of W_2 for which P_{sig} is maximized is found by setting

$$\frac{dP_{sig}}{dW_2} = 0.$$

For the case where the KE is placed at the center of the beam, $x_d = 0$, we obtain

$$\frac{d}{dW_2}\left\{\frac{\Delta x}{W_2}\exp\left[-\frac{1}{2}\left(\frac{\Delta x}{W_2}\right)^2\right]\right\} = \left[1-\left(\frac{\Delta x}{W_2}\right)^2\right]\exp\left[-\frac{1}{2}\left(\frac{\Delta x}{W_2}\right)^2\right] = 0,$$

leading to

$$W_2 = \Delta x. \quad (21)$$

This condition may be understood in terms of either the geometrical or Fresnel models of the KE technique. Consider first the Fresnel diffraction pattern of Fig. 5 with the KE obstructing the negative x_2 half plane, say. The signal power for this case is a function of the overlap between the $q = +1$ and $q = -1$ orders. For a fixed value of Δx, both the overlap of the $q = 0,+1$ orders and

that of the $q = +1,-1$ orders are error functions of W_2. The $q = +1,-1$ order overlap is, however, offset by $2\Delta x$, and consequently the signal power is maximized for $W_2 = \Delta x$.

The geometrical interpretation is best described when the far-field approximation of W_2 [derived from Eq. (10a)],

$$W_2 = \frac{\lambda z}{\pi W_1},$$

and the expression for $\Delta x = \lambda/\Lambda z$ are both substituted in Eq. (21). A new condition for maximal signal power in terms of the beamwidth on the surface given by

$$W_1 = \Lambda/\pi \tag{21a}$$

is thereby obtained. This result may be interpreted in the following way. If the beam spot width W_1 were divided into small elements, the far-field electrical field may be regarded as the superposition of the electrical field amplitudes of each element. Condition (21a) indicates that as long as $W_1 \leq \Lambda/\pi$, the contribution of all the elements add in-phase, whereas, if $W_1 > \Lambda/\pi$, some of the elements produce out-of-phase electronic field amplitudes reducing the overall signal power.

Intuitively one might expect the limiting spot width for in-phase electrical field amplitude addition to be $W_1 \leq \Lambda/2$, because the surface tilt throughout half of a wavelength has the same sign. Indeed this is the condition obtained for a uniformly illuminated square spot on the surface.[2] The somewhat reduced limiting width of Eq. (21a) is attributed to the gradual decay of the optical power in Gaussian spot in contrast to the sharply defined boundary of the uniform square spot.

V. KE Technique for Nonsinusoidal SAW

The diffraction pattern derived in Sec. II assumes an infinite surface corrugation, which is associated with continuous single-frequency acoustic wavesforms. However, in many practical applications SAW pulses are employed. It is the purpose of the present section to consider the effect of nonsinusoidal SAW on the detected signal in the KE technique.

An arbitrary surface acoustic waveform, $\delta(x,t)$, may be represented as a Fourier series in spectral components,

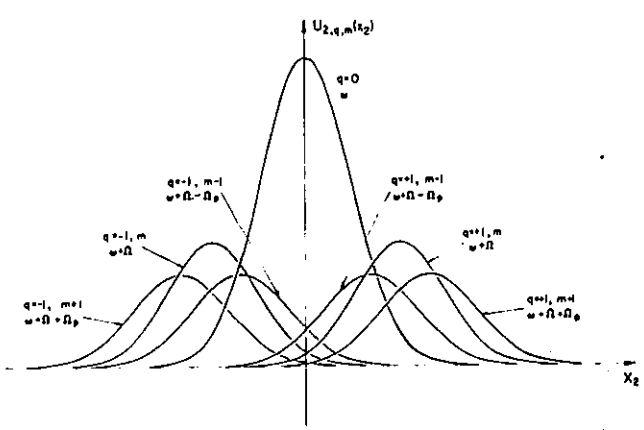

Fig. 7. Fresnel diffraction pattern for light diffracted by nonsinusoidal SAW for $W_1 \ll \Lambda_p$.

$$\delta(x,t) = \sum_{m=1}^{\infty} \delta_m \sin[m(\kappa_p x - \Omega_p t - \psi_m)], \tag{22}$$

where δ_m is the amplitude of the $m\Omega_p$ frequency component. Normally Ω_p refers to the pulsed repetition rate (PRF) in a multiple pulsed system or, alternatively, to the reciprocal of the pulse duration T_p if only one pulse is present, that is, $\Omega_p = 2\pi/T_p$. Similarly, $\kappa_p = 2\pi/X_p$, where X_p is the spatial period or spatial pulse duration for the same instances, respectively. The phase ripple modulation introduced in a beam reflected from such perturbations may be represented by

$$t(x,t) = R \prod_{m=1}^{\infty} \exp[i2k\delta_m \sin[m(\kappa_p x - \Omega_p t - \psi_m)]]. \tag{23}$$

Applying identity (5) yields

$$t(x,t) = R \prod_{m=1}^{\infty} \sum_{q_m=-\infty}^{\infty} J_{q_m}(2k\delta_m) \exp[imq_m(\kappa_p x - \Omega_p t - \psi_m)]. \tag{24}$$

Equation (24) may be multiplied out term by term producing q^m terms, which, as shown in Ref. 12, may be written as an infinite sum over a new index M. It would then be possible to perform the Fresnel integration on each of these terms to obtain an expression for the resulting near-field diffraction pattern.[5] Alternatively, the analysis may be considerably simplified if the Bessel functions of orders $q > 1$ and their multiples are neglected, as before, reducing Eq. (24) to

$$t(x,t) = R \sum_{q=-1}^{1} \sum_{m=1}^{\infty} J_q(2k\delta_m) \exp[imq(\kappa_p x - \Omega_p t - \psi_m)]. \tag{25}$$

Following a derivation similar to that which previously led from Eq. (6) to the final result of Eq. (11) for each term of the transmission function in Eq. (25), we obtain the approximate expression

$$U_2(x_2,y_2,t) = \mathrm{RE}_0 \frac{W_0}{W_2} \sum_{q=-1}^{1} \sum_{m=1}^{\infty} U_{2,q,m}(x_2,y_2,t), \tag{26}$$

where

$$U_{2,q,m}(x_2,y_2,t) = J_q(2k\delta_m) \exp\left\{-\frac{1}{W_2^2}[(x_2 - mq\Delta x)^2 + y_2^2] + \frac{ik}{2r_2}(x_2^2 + y_2^2) + imqg\left[x_2 - mq\frac{\Delta x}{2}\right]\right\} \times \exp[-i(mq\Omega_p + \omega)t - imq\psi_m + i\Phi]. \tag{26a}$$

The resulting diffraction pattern for nonsinusoidal SAW under these approximations is shown schematically in Fig. 7.

As in the case of sinusoidal SAW, the central order ($q = 0$) at frequency ω heterodynes with each of the $2m$ orders at frequencies $\omega + mq\Omega_p$ to produce rf signals at $mq\Omega_p$. The rf signals resulting from the mth order for $q = +1$ and those resulting from the mth order for $q = -1$ are both at a frequency $m\Omega_p$, but the respective phases of each signal are 180° apart. Therefore, unless a KE is introduced to block a larger portion of the mth

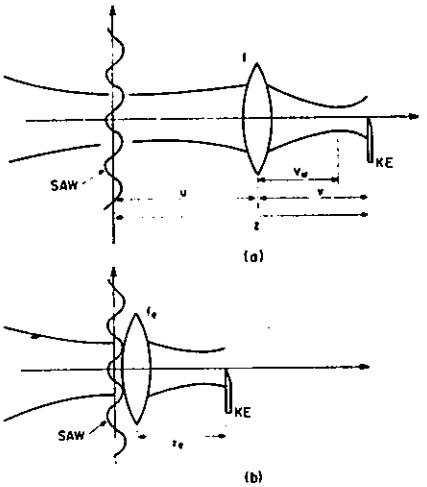

Fig. 8. Actual (a) and equivalent (b) optical systems for a KE behind a lens. (For clarity the incident beams are drawn from the left.)

order for $q = -1$, say, these signals cancel each other.

By repeating the analysis of Sec. III for the nonsinusoidal diffraction pattern of Eq. (26), it is found that

$$P_{2,rf}(x_2,y_2,t) = \frac{2R^2P_0}{\pi W_2^2}\,[U_{2,0,m}U^*_{2,1,m} + U_{2,0,m}U^*_{2,-1,m} + \text{c.c}], \tag{27}$$

where

$$U_{2,0,m}U^*_{2,q,m}|_{q=\pm1} = J_1(2k\delta_m)\exp\left\{-\frac{1}{W_2^2}\,[x_2^2 + (x_2 - mq\Delta x)^2 + 2y_2^2] - imqg\left(x_2 - mq\frac{\Delta x}{2}\right)\right\} \times \exp(+imq\Omega_p t + imq\psi_m) \tag{27a}$$

The signal power may be found by integrating this rf component of the irradiance over the area of the unblocked detector [Eq. (18)], resulting in

$$P_{sig}(x_d,t) = \sqrt{\frac{2}{\pi}}\frac{R^2P_0}{W_2}\sum_{m=1}^{\infty} J_1(2k\delta_m)\mathcal{J}'_{sig}(m,x_d,t), \tag{28}$$

with

$$\mathcal{J}_{sig}(m,x_d,t) = \int_{x_d-m\Delta x/2}^{x_d+m\Delta x/2}\exp\left[-\frac{1}{2}\left(m\frac{\Delta x}{W_2}\right)^2\right]\exp\left[-2\left(\frac{x}{W_2}\right)^2\right] \times \cos(m\Omega_p t + m\psi_m - mgx)dx. \tag{28a}$$

For small Δx, Eq. (28) may be approximated by

$$P_{sig}(x_d,t) \simeq \sqrt{\frac{2}{\pi}}\frac{R^2P_0}{W_2}\exp\left[-2\left(\frac{x_d}{W_2}\right)^2\right]\sum_{m=1}^{\infty} m\Delta x k\delta_m \times \exp\left[-\frac{1}{2}\left(m\frac{\Delta x}{W_2}\right)^2\right] \times \cos(m\Omega_p t + m\psi_m - mgx_d), \tag{29}$$

where the small argument Bessel function approximation, $J_1(x) = \frac{1}{2}x$, was introduced in the last step.

The term

$$\exp\left[-\frac{1}{2}\left(m\frac{\Delta x}{W_2}\right)^2\right]$$

in Eq. (29) describes the bandpass filtering quality of the knife-edge technique where both large and small m orders are detected with reduced amplitudes. This is a consequence of the dependence of the signal power on the ratio $m\Delta x/W_2$. (In Sec. IV it was shown that the maximal signal is obtained when $W_2 = m\Delta x$.) On defining

$$B = \exp\left[-\frac{1}{2}\left(m\frac{\Delta x}{W_2}\right)^2\right],$$

letting $x_d = 0$, substituting for Δx, and introducing the relation

$$\frac{1}{\Lambda_p} = \frac{\Omega_p}{2\pi V},$$

where V is the acoustic velocity, Eq. (29) reduces to

$$P_{sig}(t) \simeq \sqrt{\frac{2}{\pi}}\frac{R^2P_0}{W_2}\sum_{m=1}^{\infty}\frac{B}{V}m\Omega_p\delta_m\cos[m\Omega_p t + \psi_m)]. \tag{30}$$

This expression is approximately proportional to the temporal variation of the surface slope,

$$\frac{d}{dt}\,[\delta(x_1 = 0,t)],$$

provided that, for all m for which the magnitude of δ_m is significant, both B is approximately constant (the acoustic frequency bandwidth is sufficiently small) and V is approximately constant (no acoustic dispersion).

VI. Knife-Edge Behind a Lens

The treatment in the previous sections referred to the simplified KE system of Fig. 1. In practical KE systems, however, a lens is normally placed in the reflected optical beam path Fig. 8(a)], for which the results so far do not hold. Nevetheless, it is possible to show that the system of Fig. 8(a) is optically equivalent to the system of Fig. 8(b), where the lens f is replaced by aneffective lens f_e positioned in the optical beam path immediately after the reflection from the SAW surface, provided that

$$z_e = z - \frac{u}{f}v, \qquad f_e = \frac{z}{v}f - u = z_e f/v,$$

a quadratic phase correction ϕ_e is applied to the KE plane, and the apertures of both systems are infinite. This claim may be verified either by employing the basic Vander Lugt equation[13] or by applying repeatedly the Fresnel integral to calculate the output optical distribution function of both systems.[5]

Using this model it is possible to modify the expression for the signal power in the simple KE system [Eq. (17)] to describe the signal power for the standard KE system of Fig. 8(b). The phase correction ϕ_e does not affect the results and is lost when the conjugate multiplication [in Eq. (14)] is carried out. Therefore, the required expression is identical to Eq. (17) if W_2 is replaced by W_e, g by g_e, and z by z_e, and when it is remembered that the initial phase curvature $1/r_{1e}$ must now include the phase curvature introduced by the lens f_e. Thus

$$P_{sig}(x_d,t) = \sqrt{\frac{2}{\pi}}\frac{1}{W_e} J_0 J_1 R^2 P_0 \exp\left[-\frac{1}{2}\left(\frac{\Delta x_e}{W_e}\right)^2\right] \times \int_{x_d-\Delta x_e/2}^{x_d+\Delta x_e/2} dx \exp\left[-2\left(\frac{x}{W_e}\right)^2\right] \times \cos(\Omega t + \psi - g_e x), \quad (31)$$

where

$$x_e = \frac{\lambda}{\Lambda} z_e, \quad (31a)$$

$$W_e = W_1\sqrt{\zeta_e^2 + z_e^2/Z^2}, \quad (31b)$$

$$\zeta_e = 1 + z_e/r_{1e}, \quad (31c)$$

$$Z = (\pi W_1^2)/\lambda, \quad (31d)$$

$$\frac{1}{r_{1e}} = \frac{1}{r_1} - \frac{1}{f_e}, \quad (31e)$$

$$\frac{1}{r_e} = \frac{1}{z_e}\left[1 - \frac{\zeta}{\zeta^2 + (z_e/Z)^2}\right], \quad (31f)$$

$$g_e = \kappa(1 + z_e/r_e). \quad (31g)$$

For small Δx_e, Eq. (31) may be approximated by

$$P_{sig}(x_d,t) \simeq \sqrt{\frac{2}{\pi}}\frac{x_e}{W_e} J_0 J_1 R^2 P_0 \exp\left[-\frac{1}{2}\left(\frac{x_d}{W_e}\right)^2\right] \times \cos(\Omega t + \psi - g_e x_d). \quad (32)$$

Several phenomena are predicted by Eqs. (31) and (32). When $z_e = -r_e$ (which for $r_1 = \infty$ implies $z_e = f_e$ or $v = f$) it is found from Eq. (31) that $g_e = 0$, and the signal phase becomes independent of x_d. The condition $v = f$ occurs when the KE is placed at the back focal plane of the lens. As in this plane the far-field is formed (Fourier transform plane), the condition of no signal phase dependence on x_d in the far-field limit is reconfirmed.

At the point where $z_e = -r_{1e}$, g_e changes sign from positive for $z_e < f_e$ to negative for $z_e > f_e$. This sign change is predicted by geometrical considerations. (A KE on the left side of the beam produces a signal in-phase opposition to a KE on the right side of the beam. After the focal point, $v = f$, the left and right sides of the beam are interchanged.) This phenomenon is demonstrated in the results of experimental work, which are described in the next section.

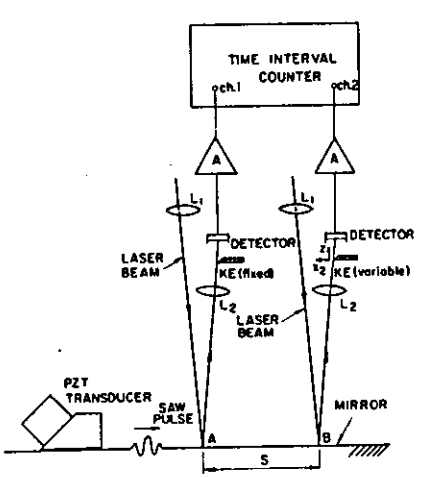

Fig. 9. Schematic illustration of the experimental apparatus.

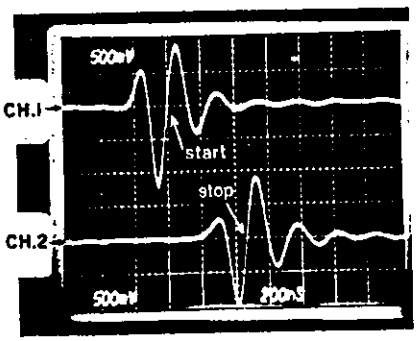

Fig. 10. Oscilloscope traces of the two amplified and detected acoustic signals.

Note that the inflection point where g_e changes sign is the focal plane $v = f$ and not the beam waist point, which is easier to locate in a KE experiment. Differentiation of Eq. (31b) results in the useful expression

$$v_w = \frac{Z^2 - u(f-u)}{Z^2 + (f-u)^2} f, \quad (33)$$

from which we conclude that $v_w < f$ for $u < f$ and vice versa. Only when $u = f$ does the focal plane coincide with the plane defined by the beam's waist.

VII. Experimental

The theoretical dependence of the detected acoustic signal phase on the KE position was verified experimentally by employing two similar SAW detecting stations as illustrated in Fig. 9. A piezoelectric transducer was used to generate SAW pulses of 5-MHz center frequency on the front face of an optical mirror. Each acoustic pulse was at first detected at point A on the mirror surface by the KE system of Ch. 1 and then at point B on the mirror surface by the KE system of Ch. 2. The amplified electronic signals obtained in the two channels (Fig. 10) were fed into Ch. 1 (START) and Ch. 2 (STOP) of a time interval counter, which was programmed to initiate the measurement at the first positive slope zero crossing of the signal on Ch. 1 and terminate the measurement at the corresponding point on the signal of Ch. 2 (see Fig. 10). The KE of Ch. 1 was maintained fixed, while that of Ch. 2 was scanned across the optical beam (along the x_2 direction), and the time interval between the signals of Ch. 1 and Ch. 2 was measured as a function of x_2. This procedure was repeated for several positions along the optical beam axis (z axis). The measurements along this axis are taken relative to the position of the narrowest portion of the optical beam (beam's waist), which was found by searching for the position along the z axis for which the noise level in the detector, indicating the presence of the laser light, persisted for the minimal scan along x_2. The experimental results are plotted in Fig. 11. Figure 12 shows the theoretical dependence of the signal phase on x_d as predicted by Eq. (36).

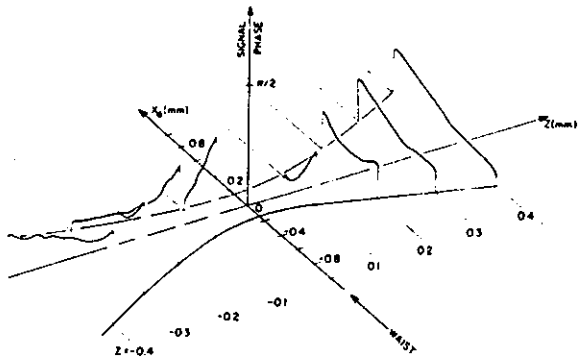

Fig. 11. Experimental variation of signal phase with KE position.

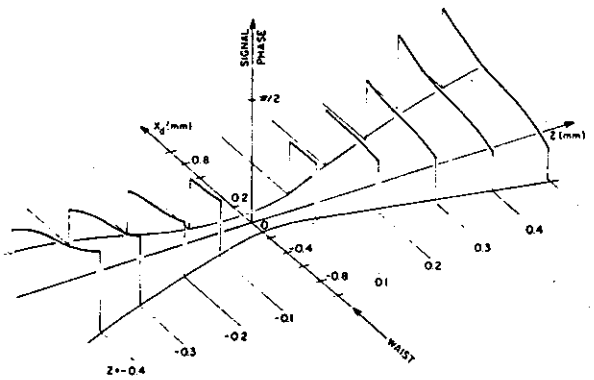

Fig. 12. Theoretical variation of signal phase with KE position.

VIII. Discussion

There is a good agreement between the variation of the signal phase with the KE position as measured experimentally (Fig. 11) and that predicted by the numerical integration of the theoretical results (calculated for $r_1 = \infty$, $W_1 = 0.2$ mm, $f = 50$ mm, $z = 650$ mm, and $u = 0$ and shown in Fig. 12). The slopes of the signal phase before and after the narrowest beam point (the origin in the graphs of Figs. 11 and 12) have been correctly predicted. The lapsed time was found to increase as the KE of Ch. 1 placed before the focal point is drawn transversely to the beam and away from the KE of Ch. 2. These results support the physical interpretation given in Sec. III, whereby the KE is considered to define through partial imaging a small region within the illumination spot on the SAW surface. As the KE is moved in the said direction, the effective separation along the SAW propagating surface between the two KE-stations is increased, and the measured lapsed time increases with it.

Other similarities between the theoretical and experimental graphs are less significant as the parameters used for the theoretical calculations are difficult to measure. Nevertheless, it is noted that the correct order of magnitude for the phase gradient g is predicted by the theory. Moreover, the position of the Fourier (focal) plane, which is determined in our analysis to coincide with the position along the z axis where the signal phase is constant as a function of x_d, occurs in both graphs at $z \simeq 0.2$ mm.

These results demonstrate the importance of the understanding and control of the phase detection in the KE technique when an accurate definition of the beam spot is required as is the case for SAW velocity measurements by the time-of-flight method.[5] Indeed our experimental system, described in Fig. 9, achieved SAW velocity measurement accuracies of $(\Delta V)/V = 10^{-4}$ and better.[14]

IX. Conclusion

The KE technique is analyzed by Fresnel diffraction methods both for continuous and pulsed SAW. The analytical expressions obtained for the detected signal describe in both cases a dependence of the detected signal phase on the lateral position of the KE. Intuitively this phenomenon is interpreted as resulting from the partial imaging occurring between regions on the SAW-propagating surface and the KE plane. It is demonstrated that the near-field characteristics of the KE, which have been verified experimentally, comply with the results obtained previously in the far-field. Other results include an analytic description of the technique with any lens system and the relation between the signal amplitude and illumination spot width. The generality of the results described herein permits prediction of the performance of experimental instrumentation employing the KE technique under a wide range of operating conditions. Full understanding and control of the detected signal phase in the KE technique are important for any application requiring phase accuracy, such as SAW time-of-flight measurements.

References

1. H. Engan, "Phase Sensitive Probe for High-Frequency Surface Acoustic Wave Measurements," IEEE Trans. Sonics Ultrason. SU-25, 372 (1978).
2. R. L. Whitman and A. Korpel, "Probing of Acoustic Surface Perturbations by Coherent Light," Appl. Opt. 8, 1567 (1969).
3. G. I. Stegeman, "Optical Probing of Surface Waves and Surface Wave Devices," IEEE Trans. Sonics Ultrason. Su-23, 33 (1976).
4. C. H. Palmer and R. E. Green, Jr., "Optical Probing of Acoustic Emission Waves," in *Twenty-third Sagamore Army Materials Research Conference on Nondestructive Characterization of Materials*, Raguette Lake, N.Y. (1976), p. 347.
5. A. Aharoni, "An Optical Probe for SAW velocity Measurements," MSc. Thesis, Tel Aviv U. (1983).
6. W. H. Southwell, "Validity of the Fresnel Approximation in the Near Field," J. Opt. Soc. Am. 71, 7 (1981).
7. A. Yariv, *Introduction to Optical Electronics* (Holt, Rinehart & Winston, New York, 1971).
8. H. Kolsky, *Stress Waves in Solids* (Dover, New York, 1952).
9. J. W. Goodman, *Introduction to Fourier Optics* (McGraw-Hill, New York, 1968).
10. I. S. Gradshteyn and I. M. Ryzhik, *Tables of Integrals Series and Products*, (Academic, New York, 1965).
11. R. J. Hallermeier and W. G. Mayer, "Frequency Shifting of a Gaussian Light Beam by Ultrasonic Surface Waves," J. Appl. Phys. 41, 3664 (1970).
12. T. H. Neighbors III and W. G. Mayer "Asymmetric Light Diffraction From Nonsinusoidal Ultrasonic Surfaces Waves," J. Appl. Phys. 42, 3670 (1971).

13. A. VanderLugt, "Operational Notation for the Analysis and Synthesis of Optical Data-Processing Systems," Proc. IEEE 54, 1055 (1966).
14. A. Aharoni and K. M. Jassby, "Monitoring Surface Properties of Solids by Laser based SAW Time of Flight Measurements," accepted for publication, IEEE Trans. Sonics Ultrason. (June 1985).

INTERNATIONAL SYMPOSIUM ON OPTO-ELECTRONIC IMAGING December 2—5, 1985

INTERNATIONAL SYMPOSIUM ON OPTO - ELECTRONIC IMAGING

DECEMBER 2-5, 1985

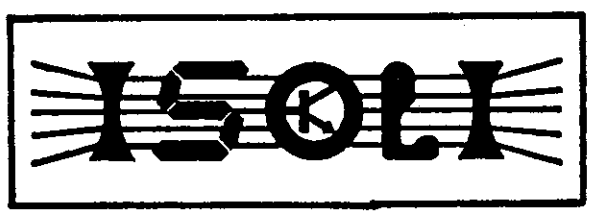

Sponsored by :
Defence Research and Development Establishment, INDIA

Organised by :
Instruments Research & Development Establishment, Dehra Dun, INDIA